含咔唑之非富勒烯受體於三元混摻有機太陽能電池中展現超過 16.6 %的光電轉換效率且無需添加劑

Carbazole-based nonfullerene acceptors enable 16.6 % PCE without additives in ternary organic solar cell

本團隊分別設計了含不同橋接原子，及側鏈改質後以咔唑為中心之非富勒烯受體 DTSiC-4Cl/DTCC-4Cl 和 DTTC-4FC8/DTTC-4ClC9。藉由優化三元混摻比例，分別展現 15.04%和 16.66%之光電轉換效率。

將噻吩以矽代替碳做為橋接原子熔合於咔唑中心兩側。由於硅雜環戊二烯相比於環戊二烯具有獨特之 σ*–π* 共軛特性，使得其受體 DTSiC-4Cl 表現出較高之 LUMO，在光伏表現上能提升開路電壓，且無須添加劑優化其排列。另外，我們將 LUMO 較高之 DTTC 系列受體導入 PM6:Y6，合理提升其開路電壓，並減少強聚集性 Y6 之用量，降低粗糙度提升填充因子，達到 16.66%之光電轉換效率。

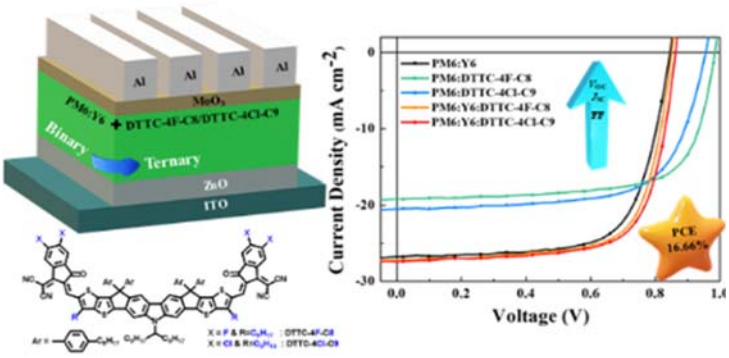

Figure: Schematic representation of the molecular design.

Two series of carbazole-based non-fullerene acceptors (NFAs), DTCC-4Cl/DTSiC-4Cl and DTTC-4FC8/DTTC-4ClC9, were designed in ternary organic solar cell, affording decent power conversion efficiency (PCE) of 15.04% and 16.66%, respectively.

The silole units embedded in DTSiC core manifest its unique σ*–π* conjugation feature, leading to the up-shifted LUMO and high V_{OC} performance in ternary OSC, exhibiting a decent PCE of 15.04% without additive. Also, DTTC-based NFAs, with higher LUMO than Y6, were introduced into PM6:Y6 host. The PM6:Y6:DTTC-4ClC9 ternary device exhibits an elevated V_{OC} of 0.86 V and PCE of 16.66% with modified morphology.

* T.-W. Chen, J.-Y. Yu, Y.-W. Lin, S.-H. Peng, S.-H. Wu, Y.-J. Su, V. K. Karapala, L. Hong, H. Yao, J. Hou, and C.-S. Hsu, "Chlorinated Carbon-Bridged and Silicon-Bridged Carbazole-Based Nonfullerene Acceptors Manifest Synergistic Enhancement in Ternary Organic Solar Cell with Efficiency over 15%", Sol. RRL, **4**, 2000357, (2020).
* J. Chen and C.-S. Hsu, Journal of Material Chemistry A, in press.

具 9.5%高效率之 20*30 平方公分有機太陽電池

Large area organic photovoltaic panel on 30 cm by 20 cm substrate with a power conversion efficiency of 9.5%

傳統的矽晶體太陽能電池浪費了暗影中的區域。而半透明的太陽能電池可使得下面的區域仍然可以使用。它們可以安裝在溫室中或作為建築物集成光(BIPV)安裝。有機光伏(OPV)或有機太陽能電池由於其半透明性和簡易製程而成為一種新興技術。在本工作中，我們發展了一種大面積且可溶液處理的有機光伏。$SiW_{12}O_{40}$ 陰極界面層平均厚度僅 10 nm。活性光吸收層平均厚度 100 nm 並且誤差在 10 nm 以下。該模組在 30 cm x 20 cm 的基板上，有效面積為 216 cm^2 的情況下實現了 9.5 %的功率轉換效率。發表時為有效面積超過 100 平方厘米 OPV 模組的最高效率。

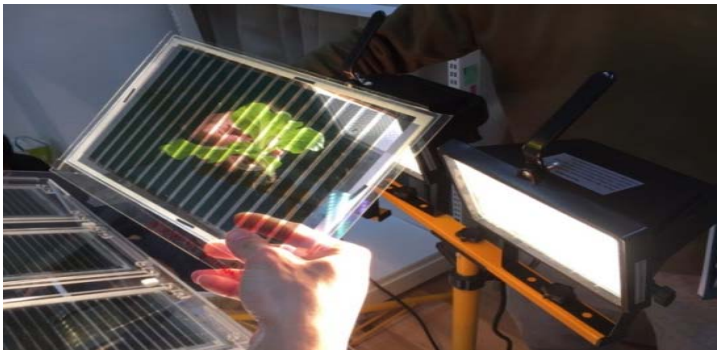

Figure: Large-area organic PV module with 9.5%.

It is desirable to have semi-transparent solar cells, such that the areas below can still be used. Organic photovoltaic (OPV), or organic solar cell, is a promising emerging technology because of its semi-transparency and easy solution process. Herein, we present a large-area and solution-processable OPV module. The active light absorbing layer is coated with mean thickness of 100 nm and variation below 10 nm. The module achieved a power conversion efficiency of 9.5% with an active area of 216 cm^2 on a 30 cm by 20 cm substrate. It is the record high efficiency by far for OPV module as it was published.

---

* C.-Y. Tsai, Y.-H. Lin, Y.-M. Chang*, J.-C. Kao, Y.-C. Liang, C.-C. Liu, J. Qiu, L. Wu, C.-Y. Liao, H.-S. Tan, Y.-C. Chao, S.-F. Horng, H.-W. Zan, and H.-F. Meng*, F. Li *, "Large area organic photovoltaic modules fabricated on a 30 cm by 20 cm substrate with a power conversion efficiency of 9.5 %", Solar Energy Materials & Solar Cells, **218**, 110762 (2020).

以新穎兩步法製備無鉛鈣鈦礦太陽能電池研究
A novel two-step approach to fabricate lead-free perovskite solar cells

傳統鉛鈣鈦礦電池可以由兩步法來製備鈣鈦礦主動層，其關鍵的第二步驟是由異丙醇(IPA)作為溶劑來達成，然而在錫鈣鈦礦的製備中，由於 IPA 會將錫鈣鈦礦腐蝕，因此錫鈣鈦礦太陽能電池都是由一步法來完成。本研究是世界上第一個用兩步法來製備錫鈣鈦礦太陽能電池的例子。我們成功開發出混溶劑，以 IPA 混六氟異丙醇(HFP)以及氯苯(CB)在 5:5:2 的比例下做為第二步的溶劑，在回火 70 度 C 條件下可以長出均勻的錫鈣鈦礦薄膜。其中在第一步驟中，我們加入添加劑 $EDAP_2$，這可以抑制二價錫氧化成四價錫，而使得元件的整體效能從 5 %提升至 7 %，且元件穩定性大為提升，在手套箱中可以維持 4000 小時而不衰退，未來這個方法可以在第一步驟中改變混參陽離子的比例、添加劑的種類，而在第二步驟改變陰離子的種類而廣泛應用到商業化的製程。

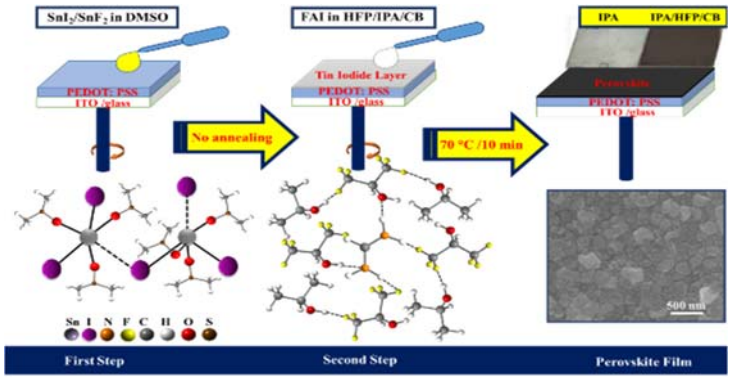

Figure: Two-step fabrication procedure.

Applying a two-step procedure and solvent engineering we fabricated a stable tin-based perovskite, formamidinium-tin-triiodide ($FASnI_3$) solar cell for lead-free photovoltaic applications. The first step was deposition of a SnI_2 layer with solvent dimethyl sulfoxide (DMSO); the second step applied a cosolvent system containing hexafluoro-2-propanol (HFP), isopropyl alcohol (IPA) and chlorobenzene (CB) in ratio 5:5:2 to deposit the FAI layer on the SnI_2 layer. The traditional IPA solvent prevented the formation of a stable $FASnI_3$ layer such that a stable device could not be fabricated. HFP was hence used to form hydrogen bonding with IPA and FAI to retard the crystal growth of $FASnI_3$; CB served as anti-solvent. Ethylenediammonium dihypophosphite ($EDAP_2$) in the first step was an effective reducing agent to increase the efficiency of power conversion from ~5 % to ~7 % with great reproducibility and stability over 4000 h. For the first time a stable $FASnI_3$ solar cell has been produced via a two-step deposition, which may provide us more flexibility to control the film quality and crystal structure, via varying halides and co-additives in the first step and co-cations and bulky organic cations in the second step, for further development of tin-based perovskite solar cells with enhanced device performance and stability.

* S. Shahbazi, M.-Y. Li, A. Fathi, and E. W.-G. Diau*, “Realizing a Cosolvent System for Stable Tin-Based Perovskite Solar Cells Using a Two-Step Deposition Approach”, ACS Energy Lett. **5**, 2508 (2020).

以機械堆疊 GaInP/GaAs 與多晶矽研製三階面太陽能電池

Triple-junction solar cells of mechanical stacked GaInP/GaAs on poly-Si

矽(Si)和 III-V 化合物多結太陽能電池集成太陽能電池已被廣泛研究，用以實現高效率太陽能電池。在本研究中，開發了一種機械堆疊技術用以將 GaInP / GaAs 和多晶矽太陽能晶片整合在一起。GaInP / GaAs /多晶矽三結太陽能電池採用低溫貼合技術進行機械堆疊，該技術使用高光透射旋塗材料將微金屬球撒到金屬線上。GaInP / GaAs /多晶矽三結太陽能電池的電流-電壓測量是使用太陽能模擬器在室溫下在暗處和 1 個陽光下以 100 mW / cm^2 的功率密度進行的。GaInP / GaAs /多晶矽三結太陽能電池的效率為 24.5 %，開路電壓為 2.68 V，短路電流密度為 12.39 mA / cm^2，填充係數為 73.8 %。

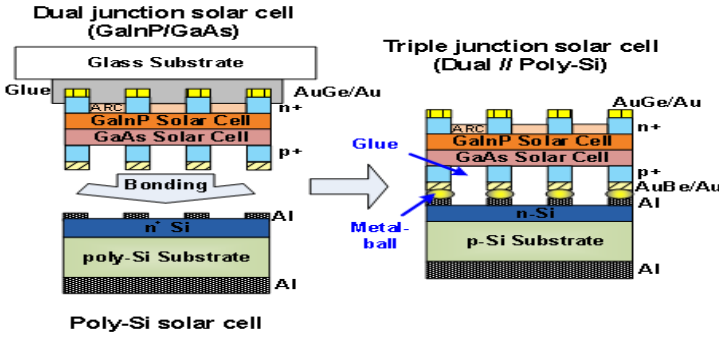

Figure: Schematic structure of the GaInP/GaAs dual-junction, poly-Si, and GaInP/GaAs//poly-Si triple-junction solar cells.

The integration of silicon (Si) and III–V compound multi-junction solar cells to function as photovoltaic devices has been widely investigated to achieve ultrahigh-efficiency performance in converting solar energy to electric power. In this study, a mechanical stacking technique is developed to bond GaInP/GaAs and poly-silicon solar wafers together. A GaInP/GaAs/poly-Si triple-junction solar cell was mechanically stacked using a low-temperature bonding process, which involves sprinkling micro metal balls onto a metal line using a high- optical-transmission spin-coated glue material. Current–voltage measurements of the GaInP/GaAs/poly- Si triple- junction solar cell were carried out at room temperature both in the dark and under 1 sun with 100 mW/cm^2 power density using a solar simulator. The GaInP/GaAs/poly-Si triple-junction solar cell reached an efficiency of 24.5 % with an open-circuit voltage of 2.68 V, a short-circuit current density of 12.39 mA/cm^2, and a fill-factor of 73.8 %.

---

* R. H. Horng, paper in preparation.

高效產氫量子點光觸媒

Highly efficient quantum dot photocatalysts for hydrogen production

諸如 CdS 和 CdSe 的二元半導體量子點已被廣泛用作光觸媒產氫，但是鎘的高毒性阻礙了它們的廣泛應用。近年來，多元合金 I-III-VI 的半導體例如 $AgInS_2$ 和 $CuInS_2$，可做為對環境無害、有前途的替代光觸媒。

在這項工作中，我們製備合金化的 ZnSe-$AgInSe_2$（ZAISe）量子點並評估其對產氫的光催化活性。通過分別控制 Zn 和 Ag 的比例，即（Ag＋In）/（Zn＋Ag＋In）和 Ag/（Ag＋In），可以對 ZAISe 量子點的能帶結構進行微調以改善其光催化活性。ZAISe 的光催化反應的作用譜顯示在 400 至 700 nm 的整個可見光區域內都具有活性。產氫的最高量子產率在 600 nm 的照光下，產率達到 3.4％。在這項工作中，我們製備合金化的 ZnSe-$AgInSe_2$（ZAISe）量子點並評估其對產氫的光催化活性。通過分別控制 Zn 和 Ag 的比例，即（Ag＋In）/（Zn＋Ag＋In）和 Ag/（Ag＋In），可以對 ZAISe 量子點的能帶結構進行微調以改善其光催化活性。ZAISe 的光催化反應的作用譜顯示在 400 至 700 nm 的整個可見光區域內都具有活性。產氫的最高量子產率在 600 nm 的照光下，產率達到 3.4％。

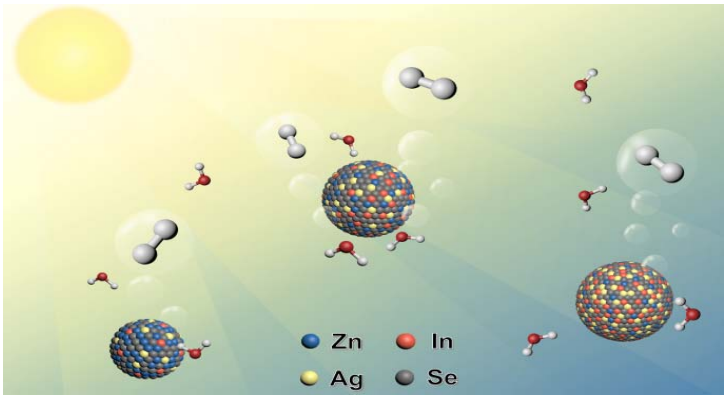

Figure: Hydrogen Production on ZnSe-$AgInSe_2$.

Binary semiconductor quantum dots such as CdS and CdSe have been widely studied as photocatalysts for hydrogen production, but the high toxicity of Cd impedes their widespread deployment. Recently, multinary I–III–VI-based semiconductors, e.g., AgInS2 and CuInS2, have emerged as promising alternatives for environmentally benign photocatalysts.

In this work, we prepared quantum dots (QDs) composed of an alloyed ZnSe–AgInSe2 (ZAISe) and evaluated their photocatalytic activity for H2 production. By individually controlling the fractions of Zn and Ag, that is, the ratios of (Ag + In)/(Zn + Ag + In) and Ag/(Ag + In), the band structure of ZAISe QDs could be finely tuned to improve their photocatalytic activity. The highest apparent quantum yield of H2 production reached 3.4 % under irradiation at 600 nm.

* P.-Y. Hsieh, T. Kameyama, T. Takiyama, K. Masuoka, T. Yamamoto, Y.-J. Hsu*, and T. Torimoto*, “Controlling the visible-light driven photocatalytic activity of alloyed ZnSe-$AgInSe_2$ quantum dots for hydrogen production”, J. Mater. Chem. A, **8**, 13142 (2020).

以可光轉換高分子與超分子作用力做為離子檢測之應用

Multi-stimuli responsive and efficient FRET approaches of bifluorophores toward ion detections via supramolecular interactions of photo-switchable polymers and [2]rotaxanes

幾種多刺激應答性雙螢光團可光轉換的聚合物、(近)輪烷、和主客系統被開發具四苯基乙烯(TPE)或萘二甲酰亞胺(NI)功能化予體和光致變色花菁(MC)受體曝 UV 光。經過不同光和化學可轉換刺激的組合，這些 Förster 共振能量轉移系統可以在多個狀態之間相互切換。在半水溶液中觀察到 TPE 和 MC 單元的聚集誘導發光(AIE)和 NI 單元的聚集引起螢光猝滅(ACQ)，因此發生了各種 FRET 過程以揭示這些雙螢光體系中的不同發射顏色。最有效的 FRET 程序具有最強的紅色 MC 螢光，故具吸引人的比例螢光，因此這些紅螢光 FRET 系統對特定離子感測具有很高的選擇性和敏感性，可通過 FRET-OFF 行為恢復藍色或綠色予體的螢光，顯示出優異的檢測限(LOD)值，並可用於活細胞中離子檢測的細胞成像。

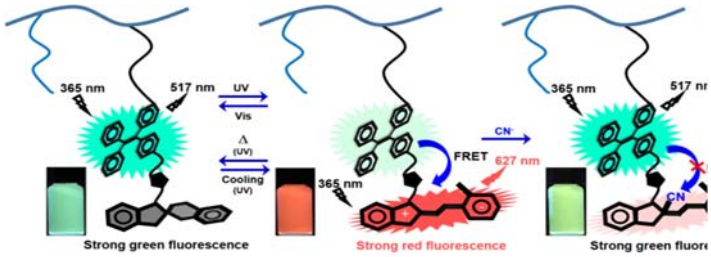

Figure: Schematic representations of multi-stimuli responsive photo-switchable FRET system.

Several multi-stimuli responsive bi-fluorophoric photo-switchable polymers, [2](pseudo-)rotaxanes, and host-guest systems with tetraphenylethylene (TPE)- or naphthalimide (NI)-functionalized donors and photochromic merocyanine (MC) acceptor after UV exposure were developed. By different combinations of chemical and photo-chemical switchable stimuli, these Förster resonance energy transfer (FRET) systems could be interconverted between multiple states. The aggregation-induced emission (AIE) of TPE and MC units and aggregation-caused quenching (ACQ) of NI unit were observed in semi-aqueous solutions, so various FRET processes occurred to reveal different emission colors in these bi-fluorophoric systems.

The most effective FRET process with the strongest red MC emission possessed the attractive ratiometric PL, so these red-emissive FRET systems showed high selectivities and sensitivities toward specific ion sensing to recover the blue or green donor emissions via FRET-OFF behavior, which showed excellent limit of detection (LOD) values and were utilized for the cellular imaging of ion detections in living cells.

* T. T. K. Cuc, P. Q. Nhien, T. M. Khang, C. C. Weng, C. H. Wu, B. T. B. Hue, Y. K. Li, J. I. Wu, and H. C. Lin*, "Optimization of FRET behavior in photo-switchable [2]rotaxanes containing bi-fluorophoric naphthalimide donor and merocyanine acceptor with sensor approaches toward sulfite detection", Chem. Mater. **32**, 9371 (2020).

* P. Q. Nhien, W. L. Chou, T. T. K. Cuc, T. M. Khang, C. H. Wu, N. Thirumalaivasan, B. T. B. Hue, J. I. Wu, S. P. Wu, and H. C. Lin*, "Multi-stimuli responsive FRET processes of bifluorophoric AIEgens in an amphiphilic copolymer and its application to cyanide detection in aqueous media", ACS Appl. Mater. Interfaces, **12**, 10959 (2020).

* P. Q. Nhien, T. T. K. Cuc, T. M. Khang, C. H. Wu, B. T. B. Hue, J. I. Wu, B. W. Mansel, H. L. Chen, and H. C. Lin*, "Highly efficient Förster resonance energy transfer modulations of dual-AIEgens between a tetraphenylethylene donor and a merocyanine acceptor in photo-switchable [2]rotaxanes and reversible photo-patterning applications", ACS Appl. Mater. Interfaces, **12**, 47921 (2020).

* F. C. Ho, Y. J. Huang, C. C. Weng, C. H. Wu, Y. K. Li, J. I. Wu, and H. C. Lin*, "Efficient FRET approaches toward copper(II) and cyanide detections via host-guest interactions of photo-switchable [2]pseudo-rotaxane polymers containing naphthalimide and merocyanine moieties", ACS Appl. Mater. Interfaces, ASAP (2020).

以呼出氣體成分建立智慧預測肺癌的模型
Lung cancer prediction using breath volatile organic compounds

人類呼出氣體中所含的揮發性有機化合物，可以反映疾病引起的代謝變化，並可以作為檢測肺癌的生物標誌物。本研究利用選擇離子流動管質譜技術，定量分析了 148 例肺癌患者和 168 名健康志願者的呼吸樣品中 123 種揮發性有機化合物的含量。我們使用機器學習方法：極端梯度增強算法，建立了一個預測模型，該模型使用揮發性有機化合物的含量來預測肺癌的疾病狀態。

我們所提出的預測模型取得了比其他先前方法更好的性能，其準確性，敏感性，特異性和 AUC 分別為 0.89、0.82、0.94 和 0.95。當進一步考慮環境有機化合物的影響時，我們可以改善模型的性能達到 0.91 的準確度，0.93 的靈敏度，0.88 的特異性和 0.98 的 AUC。

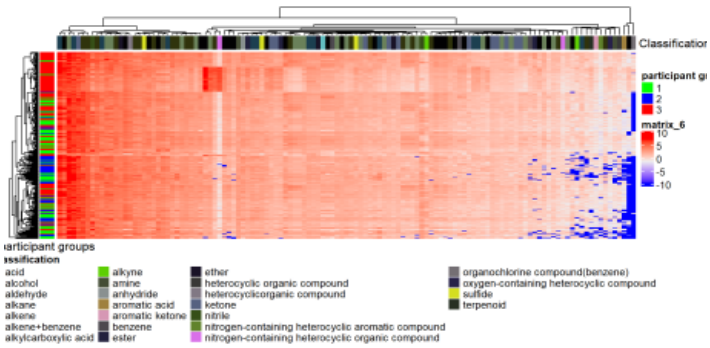

Figure: The heat map of 123 VOCs for 316 participants.

Volatile organic compounds (VOCs) derived from human breath can reflect metabolic changes caused by diseases and serve as biomarkers to detect lung cancer. The selected ion flow tube mass spectrometry technique was used to quantitatively analyze 123 VOCs in breath samples from 148 patients with histologically confirmed lung cancers and 168 healthy volunteers. We used the eXtreme Gradient Boosting (XGBoost), a machine learning method, to build a prediction model that used VOC measurements to predict lung cancer's disease state. The proposed prediction model achieved better performance than other previous approaches did, with accuracy, sensitivity, specificity, and AUC being 0.89, 0.82, 0.94, and 0.95, respectively. When further considering the environmental VOCs' effect, our model can be improved to reach a 0.91 accuracy, 0.93 sensitivity, 0.88 specificity, and 0.98 AUC.

* P. H. Tsou, Z.-L. Lin, G.-H. Huang, and Y.-K. Li, “Lung cancer prediction using breath volatile organic compounds from selected ion flow tube mass spectrometry”, (in preparation).

全球首例以影像和深度學習建立感染性角膜炎輔助診斷

Computer-aided pathogenic diagnosis of microbial keratitis on deep learning techniques

本研究提出全球首個結合眼表影像與深度學習技術之感染性角膜炎輔助診斷技術。針對感染性角膜炎之診斷靈敏度(Sensitivity)高於由三位眼科專科醫師組成之多數決診斷結果(71 % vs. 52 %)；對於黴菌性角膜炎之診斷，國外眼科醫師的臨床診斷靈敏度約 38%，特異度約僅 45 %，即便是角膜專家醫師，影像診斷的正確性也只有 66 %。因此目前此感染性角膜炎診斷效能已達眼科專科醫師之診斷正確性。

感染性角膜炎是一種嚴重威脅視覺的重大感染性眼疾，主要致病菌包括人類疱疹病毒、細菌、黴菌、棘狀阿米巴以及微孢子蟲。早期正確診斷導入精準治療是避免眼盲之關鍵，高端醫療基礎結合 AI 軟硬體發展優勢是當前國家開拓醫療科技之重點，故本研究對社會、經濟、以及學術發展各個層面之高度影響。

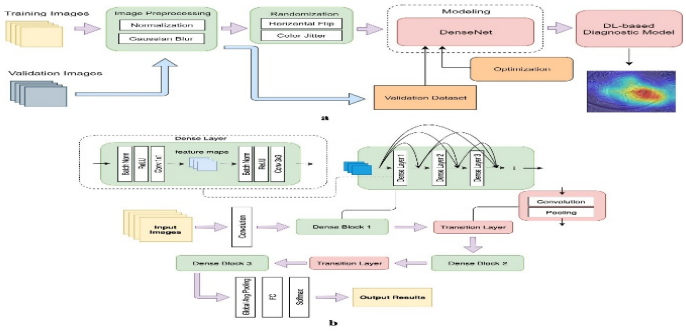

Figure: The microbial keratitis diagnosis framework.

This research is the first study that used ocular surface digital images with deep learning techniques to develop the computer-aided diagnosis system. The sensitivity of this model has achieved 71 %, which is higher than the diagnosis by three ophthalmologists (around 52 %) as well as by foreign ophthalmologists.

Microbial keratitis (MK) is a serious infectious eye disease that threatens the vision. Early diagnosis and introduction of precise treatment is the key to avoid blindness. The combination of high-end medical infrastructure and the advantages of AI software and hardware development is the current focus of the country's development of medical technology. Therefore, this research has a high impact on all aspects of society, economy, and academic development.

* M. T. Kuo, B. W. Y. Hsu, and V. S. Tseng, et al. "A deep learning approach in diagnosing fungal keratitis based on corneal photographs", Sci. Rep. **10**, 14424 (2020).

抗沾黏胜肽晶片用於感測血液中之生物指標

An antifouling peptide-based biosensor for determination of biomarkers in human serum

常用在生物感測器中的生物辨識分子有酵素、抗體和胜肽。其中，胜肽相對酵素與抗體，具有合成容易、穩定性佳、適合後續化學修飾等優點。但其低選擇性與低親和力，是亟須克服的問題。本篇研究以多價結合力的概念，發展高變勢力、高親和力且具有抗沾黏特性之晶片。

我們透過電沉積修飾方法將四級銨鹽和硫酸根離子兩個分子組成的抗沾黏層高密度的修飾在晶片上。之後再將可辨識肺炎鏈球菌之胜肽(S7)以同樣技術修飾於晶片上已進行生物指標成分(β-內醯胺酶)之感測。結果顯示，此策略能降低生物沾黏，大幅提升生物感測的靈敏度和專一性，並展示此晶片能於 25 %的血液中完成感測分析。

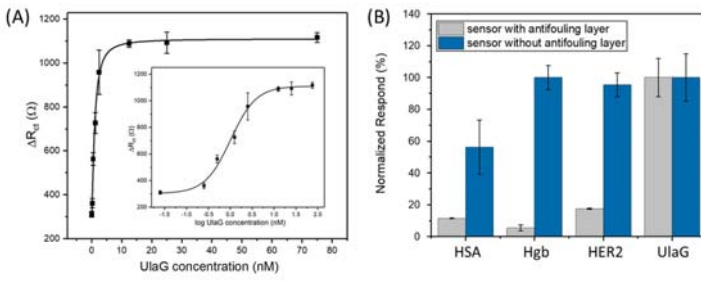

Figure: (A) Test on different concentrations of UlaG, (B) Various proteins tested on the biosensor with or without antifouling treatment.

We report a peptide-based sensor that involves a multivalent interaction with UlaG, an Streptococcus pneumonia biomarker. By integrating the antifouling feature of the sensor, we improved the S/N ratio of UlaG sensing. The antifouling layer was fabricated via electrodeposition. The aniline-modified S7 peptide, an UlaG-binding peptide, was electrochemically modified to bind onto the antifouling layer. Bio- analysis confirms that the antifouling S7-peptide sensor binds strongly to the UlaG with a dissociation constant (Kd) = 0.5 nM specifically. To show the potential for clinical application, detection of S. pneumonia from 50 to 5×104 CFU/mL were successfully performed in 25 % human serum.

* P.-H. Chang, C.-C. Weng, B.-R. Li*, and Y.-K. Li*, “An antifouling peptide-based biosensor for determination of Streptococcus pneumonia markers in human serum. Biosensors and Bioelectronic”, **151**, 111969 (2020).

開發腫瘤細胞濃縮晶片於肺癌臨床上之使用

Rapid purification of lung cancer cells in pleural effusion through spiral microfluidic channels for diagnosis improvement

近年研究發現，在癌症患者血液中發現的 CTC 的計數和表徵，為癌症轉移的早期診斷和治療預後提供了潛在的可利用資訊。然而實際上在血液中檢測 CTC 容易因其與紅血球數量相差懸殊受到嚴重干擾。

我們成功利用模擬找到最佳的聚焦及分離參數，並利用最佳化後的系統，在 10 分鐘內完整預濃縮出癌細胞。階差式串聯螺旋微流體設備是具有高通量，低製造成本，非交叉污染及有利於臨床樣品快速預處理及濃縮等優點，並且為第一個以高度差進行設計的螺旋微流體中置，是具有潛力可被視為未來癌症診斷、預後研究與其他臨床應用的工具。

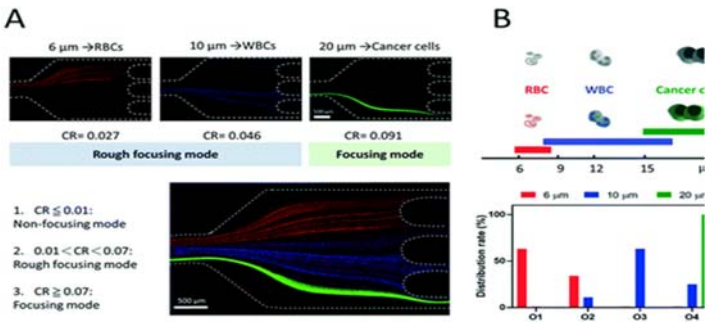

Figure: Schematic representation of the new fabrication approach.

Among cancer patients, the major reason causing the high mortality is metastasis, which means that cancer cells invade into the blood or lymph system and form new tumor(s).

We successfully optimized the system by adjusting the height of the microchannel and the input pressure, and used fluorescent microbeads and cancer cells spiked in whole blood to visualize the result and calculate the focusing and separation efficiency. In view of this, we highly expect that the CSMD device will be a crucial improvement in the field of cancer diagnosis in the near future.

* P. H. Tsou, P. H. Chiang, Z. T. Lin, H. C. Yang, H. L. Song, and B. R. Li, “Rapid purification of lung cancer cells in pleural effusion through spiral microfluidic channels for diagnosis improvement”, Lab on a Chip, **20**, 4007 (2020).
* P. L. Chiu, C. H. Chang, Y. L. Lin, P. H. Tsou, and B. R. Li, “Rapid and safe isolation of human peripheral blood B and T lymphocytes through spiral microfluidic channels”, Scientific Reports, **9**, 1 (2019).

近紅外二區螢光高分子奈米顆粒於生物顯影上應用
NIR-II fluorescent Pdots for deep-tissue imaging

在近紅外二區螢光的高分子奈米顆粒發展領域，成功開發出第一個發光在 1300 nm 波長左右的高分子奈米顆粒，因為螢光大於 1000 nm 有先物理上能隙差定律的限制，我們利用合成方法來突破並成功量產。

利用近紅外二區內的波長具有極高的組織穿透能力，在不解剖的情況下，成功應用於老鼠腦中血管顯影中，並可偵測腦中是否有血管增生的現象。

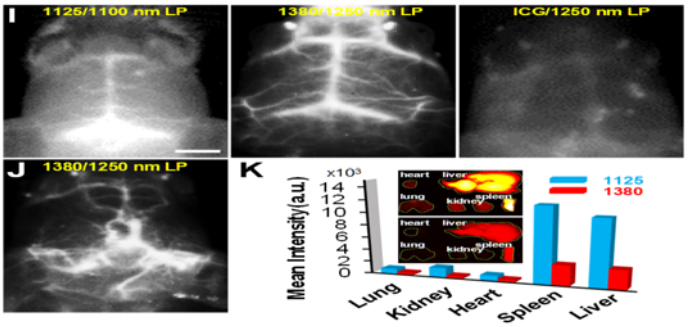

Figure: NIR-II fluorescent Pdots for bioimaging.

Deep penetration fluorescence imaging in the second near-infrared (NIR-II) window heralds a new era of clinical surgery, in which high-resolution vascular/lymphatic anatomy and detailed cancerous tissues can be visualized in real time. Although several types of fluorescent agents, including inorganic nanostructures and small organic dyes have been extensively developed recently, only a few successful examples of NIR-II fluorescing polymers with much enhanced fluorescence brightness and photo/colloidal stability have been reported. Here we describe a series of polymethine-based semiconducting polymers with intrinsic emission maxima in the NIR-IIa (1300-1400 nm) window and absorption maxima ranging from 1082 to 1290 nm. We prepared these polymers as Pdots in water with fluorescence quantum yields of 0.05-0.18 %, and demonstrated their promising applications in noninvasive through-skull brain imaging in live mice with remarkable spatial resolution as well as sig.

* M.-H. Liu, Z. Zhang, Y.-C. Yang, and Y.-H. Chan, "Polymethine-Based Semiconducting Polymer Dots with Narrow-Band Emission and Absorption/Emission Maxima at NIR-II for Bioimaging", Angew. Chem. Int. Ed. accepted (2020).

IrO_2 及 RuO_2 奈米線中的軌道多通道近藤效應

Orbital multichannel Kondo effect in Dirac nodal line IrO_2 and RuO_2 nanowires

在二氧化銥及二氧化釕金屬奈米線中，我們於低溫下觀測到由氧缺陷造成的軌道多通道近藤效應。前者的低溫電阻行為呈現了二通道近藤效應，後者的行為呈現了一通道近藤效應。兩者的低溫電阻隨溫度之變化，都不因外加磁場而改變。

我們測量液氦溫度範圍的奈米線電阻，發現在順磁性二氧化銥樣品中，電阻隨溫度下降，呈溫度的平方根方式上升。在弱反鐵磁性二氧化釕樣品中，電阻的上升則遵從一通道近藤效應之標度理論預測。外加磁場時，兩者的低溫電阻都不受影響，顯示這是一種非磁性近藤效應。我們提出理論解釋，指出造成軌道近藤效應的微觀原因在於銥和釕的最外層 d 電子軌道，存在 d_{xz} 和 d_{yz} 兩個雙重簡併態。有氧缺陷時，這雙重簡併軌道會處於半填滿狀態，與導電電子耦合，造成非費米液行為。

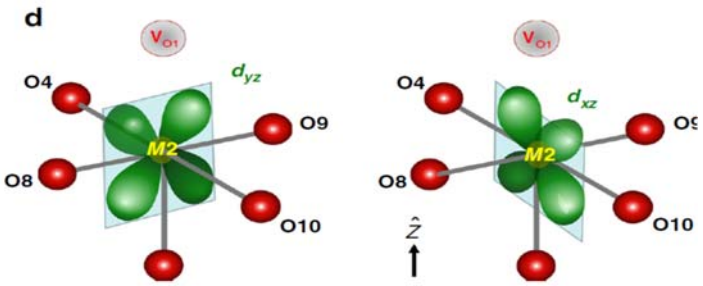

Figure: Twofold degenerate d_{xz} and d_{yz} orbitals in rutile structure.

Oxygen vacancy-driven orbital multichannel Kondo effect has been experimentally realized in Dirac nodal line metals IrO_2 and RuO_2. In paramagnetic IrO_2, two-channel Kondo effect is observed, while in antiferromagnetic RuO_2 orbital one-channel Kondo effect is found.

We have measured the low-temperature resistivities of IrO_2 and RuO_2 nanowires from 300 K down to 50 mK in zero and finite magnetic fields. In IrO_2 nanowires, the resistivity reveals a square-root-temperature increase, while in RuO_2 nanowires the resistivity conforms to a one-channel Kondo scaling form. In both cases the resistivity is insensitive to the applied magnetic field, indicating a nonmagnetic effect. The results are theoretically explained as originating from the twofold degeneracy of the half-filled d_{xz} and d_{yz} orbital in the rutile structure of IrO_2 and RuO_2.

* S. S. Yeh, T. K. Su, A. S. Lien, F. Zamani, J. Kroha, C. C. Liao, S. Kirchner, and J. J. Lin, "Oxygen vacancy-driven orbital multichannel Kondo effect in Dirac nodal line metals IrO_2 and RuO_2", Nat. Commun. **11**, 4749 (2020).

合成晶圓尺寸單晶單原子層六方氮化硼
Wafer-scale single-crystal hexagonal boron nitride monolayers on Cu (111)

二維層狀半導體材料對於半導體元件尺寸持續微縮提供了一個極具潛力的解決方案。就二維半導體元件而言，其中一項重大挑戰就是如何避免來自於鄰近介電層中的電荷散射。六方氮化硼屬於凡德瓦絕緣層，可以有效阻隔電荷散射，是一種絕佳介面介電層。然而，為了要與目前工業製程應用相容，將單晶氮化硼直接生長在晶圓上變得極為重要。

本研究成功地將單晶氮化硼以磊晶的方式生長在 2 吋藍寶石基板上的銅(111)表面。我們第一原理計算顯示氮化硼磊晶是透過銅(111)表面原子台階幫助，達成單一晶向的氮化硼，進而結合而成單晶。這個生長晶圓尺寸單晶氮化硼的可靠方法，對於未來二維電子元件的技術發展又往前邁進一步。

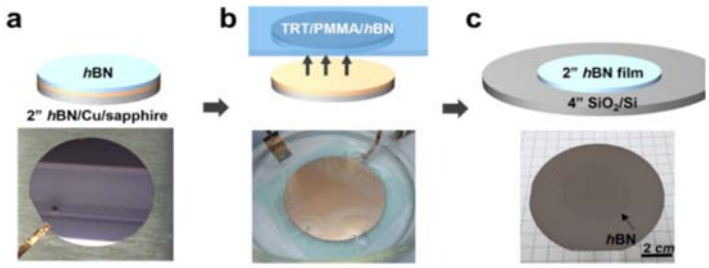

Figure: Demonstration of transferring CVD-grown 2" hBN film onto a 4" SiO_2/Si wafer.

Two-dimensional (2D) semiconducting layered materials offer great potential for continuing device scaling. One key challenge with 2D semiconductors is to avoid the charge scattering from adjacent dielectrics. An insulating van der Waals layer of hexagonal boron nitride (hBN) provides an excellent interface dielectric, efficiently reducing charge scattering. However, a reliable way of growing single-crystal hBN films directly on wafers has yet to be developed for adopting 2D layered materials in industry.

Here we report the successful epitaxial growth of single-crystal hBN monolayers on a Cu(111) film across a 2-inch sapphire wafer. Our first-principles calculations suggest that the epitaxial growth is enhanced by lateral docking of hBN to Cu (111) steps, ensuring the mono-orientation of hBN monolayers. This reliable approach to producing wafer-scale single-crystal hBN paves the way to future 2D electronics.

* T.-A. Chen, C.-P. Chuu, C.-C. Tseng, C.-K. Wen, H.-S. P. Wong, S. Pan, R. Li, T.-A. Chao, W.-C. Chueh, Y. Zhang, Q. Fu, B. I. Yakobson*, W.-H. Chang*, and L.-J. Li*, "Wafer-scale single-crystal hexagonal boron nitride monolayers on Cu (111)", Nature, **579**, 219 (2020).

凡德瓦異質結構中受莫列位能阻礙之層間激子擴散
Moiré potential impedes interlayer exciton diffusion in van der Waals heterostructures

凡德瓦異質結構的性質會受到兩層之間周期性變化的原子排列所形成之莫列超晶格影響而產生劇烈變化。激子擴散則是過渡金屬二硫族化物中能量傳遞的重要途徑之一。

本研究藉由比較分別由化學氣相沉積法與機械剝離堆疊法所製備的 $WSe_2/MoSe_2$ 雙層異質結構，我們發現因為莫列超晶格的影響而使層間激子擴散行為具有豐富的現象。我們發現莫列超晶格所的位能週期變化對於激子擴散行為會產生劇烈變化，造成完全局域、穿隧等阻礙擴散的現象。在化學氣相沉積法所製備的相稱堆疊結構中並不存在莫列超晶格，而激子擴散則顯現出最長的擴散距離。

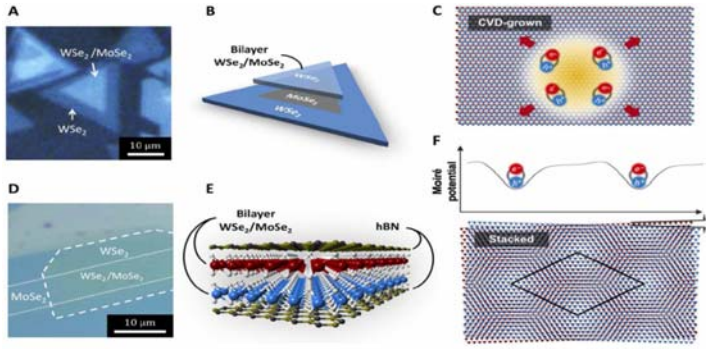

Figure: Two types of $WSe_2/MoSe_2$ heterostructures and the absence/presence of moiré superlattice.

The properties of van der Waals heterostructures are drastically altered by a tunable moiré superlattice arising from periodically varying atomic alignment between the layers. Exciton diffusion represents an important channel of energy transport in transition metal dichalcogenides (TMDs).

Here, we demonstrate the rich phenomena of interlayer exciton diffusion in $WSe_2/MoSe_2$ heterostructures by comparing several samples prepared with chemical vapor deposition (CVD) and mechanical stacking with accurately controlled twist angles. We show that the periodicity of the potential created in a moiré crystal can impact the diffusion of interlayer excitons dramatically. The diffusion is the longest in commensurate heterostructures where the moiré superlattice is completely absent.

* J. Choi, W.-T. Hsu, L.-S. Lu, L. Sun, H.-Y. Cheng, M.-H. Lee, J. Quan, K. Tran, C.-Y. Wang, M. Staab, K. Jones, T. Taniguchi, K. Watanabe, M.-W. Chu, S. Gwo, S. Kim, C.-K. Shih, X. Li*, and W.-H. Chang*, "Moiré potential impedes interlayer exciton diffusion in van der Waals heterostructures", Sci. Adv. **6**, eaba8866 (2020).

電漿電化學法合成氮摻雜二硫化鉬及洋蔥型石墨烯奈米片/二硫化鉬複合物並應用於提升產氫性質

Plasma-induced exfoliation of N-MoS_2 nanosheets and onion-like graphene-surrounded MoS_2 nanosheets for a highly efficient hydrogen evolution reaction

此研究使用電漿電化學法一步驟成功合成出氮摻雜二硫化鉬及洋蔥型結構的石墨烯奈米片與二硫化鉬複合物，並運用在提升產氫性質，其中洋蔥型結構的石墨烯奈米片/二硫化鉬複合物具有較低的 Overpotential : 118 mV (at 10 mA cm^{-2})及較低的 Tafel slope : 73 mV dec^{-1}。

以電漿電化學法中的熱離子插層進入塊材中，破壞層與層之間的反德瓦力，藉以剝離出氮摻雜二硫化鉬及洋蔥型結構的石墨烯奈米片與二硫化鉬複合物之二維材料。其中以洋蔥型結構的石墨烯奈米片/二硫化鉬複合物因其具有較多的活化表面積及較高的導電度(R_{ct}: 39 Ω)，應用在提升產氫性質具有較好的效果。

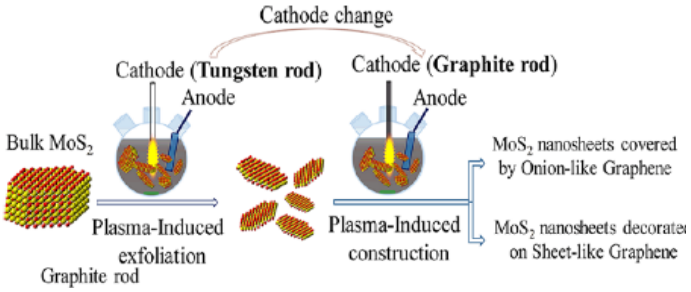

Figure: Procedure and setup for the preparation of MoS_2 nanosheets covered by graphene nanosheets.

Here we propose a facile one-pot plasma induced electrochemical process for the fabrication of N-MoS_2 and ultrathin MoS_2 nanosheets engulfed within onion-like graphene nanosheets (OGNs@MoS2). OGNs@MoS_2 composites exhibited high HER performance, characterized by a low overpotential of 118 mV at a current density of 10 mA cm^{-2}, a Tafel slope of 73 mV dec^{-1}.

We demonstrate such a facile and one-step plasma induced exfoliation approach—by cleaving of their weak out-of plane van der Waals interaction—for the production of layered N-MoS_2 nanosheets and OGNs@MoS_2 composite. The OGNs surrounding the MoS_2 not only exposed the active sites to a greater degree but also improved the conductivity (R_{ct} : 39 Ω), thereby resulting in remarkably enhanced HER activity.

* V. T. Nguyen, T. Y. Yang, P. A. Le, P. J. Yen, Y. L. Chueh, and K. H. Wei, "New Simultaneous Exfoliation and Doping Process for Generating MX2 Nanosheets for Electrocatalytic Hydrogen Evolution Reaction", ACS Appl. Mater. Interfaces, **11**, 14786-14795. (2019)
* V. T. Nguyen, T. Y. Yang, P. A. Le, P. J. Yen, Y. L. Chueh, and K. H. Wei, "Plasma-Induced Exfoliation Provides Onion-Like Graphene- Surrounded MoS2 Nanosheets for a Highly Efficient Hydrogen Evolution Reaction", ACS Appl. Mater. Interfaces, **12**, 11533-11542 (2020).

機械式可調控非線性介電體
Mechanically controllable nonlinear dielectrics

在這項研究中，由順電 BSTO，鐵電 BTO 和半導體 AZO 層組成的柔性氧化物異質外延電容器和 FeFET 在二維白雲母襯底上製備，並確定了外延關係。BSTO 電容器在機械彎曲下表現出較高的介電常數可調性（-77.8～34％）。在沒有 AZO 層的情況下，對 BTO / SRO /雲母樣品的實驗表明，在不同的彎曲半徑下 BTO 鐵電極化的幅度減小。

在 FeFET 部分中，開/關電流比可以達到 2 數量級的變化，並顯示歸因於 BTO 鐵電的逆時針 I_D-V_D 曲線。當它以 0.285 mm-1 的曲率彎曲時，其下降幅度大約等於兩個數量級。XPS 和拉曼光譜的結果也一起提供了對該機理的重要見解。我們相信，基於白雲母上異質外延的 FeFET 可以通過簡單的機械彎曲而成為靈活可調諧的電子組件。這一全新的突破為機械可調技術的未來應用提供了一條有希望的途徑。

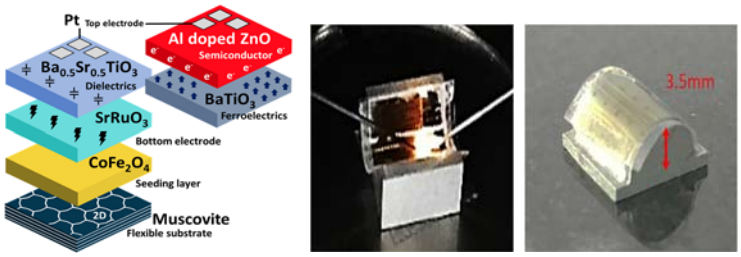

Figure: Schematic of BSTO, BTO systems and their bending states..

In the past decade, strain engineering has been used to markedly manipulate characteristics of functional materials such as increasing tunability. In this study, in order to surmount this obstacle, we adopt flexible muscovite mica substrate to fabricate epitaxial $(Ba_{0.5}Sr_{0.5})TiO_3$ (BSTO) thin films with high and tunable dielectric constant via van der Waals epitaxy. The combination of X-ray diffraction and high-resolution transmission electron microscopy was conducted to reveal the heteroepitaxy of the BSTO/muscovite system.

Due to the mechanical flexibility of muscovite sheet, the tunability of dielectric constant were highlighted by the capacitance-voltage measurement under various bending measurement. In the bending measurement, the dielectric constant of BSTO thin films with different thicknesses was altered nonlinearly and reversibly from -77 % to 36 % compared to the unbent state. Such a system composed of flexible BSTO/muscovite heteroepitaxy delivers a new path way to apply mechanical strain on thin film system with tunable dielectric feature.

---

* D. L. Ko, M. F. Tsai, J. W. Chen, P. W. Shao, Y. Z. Tan, J. J. Wang, S. Z. Ho, Y. H. Lai, Y. L. Chueh, Y. C. Chen, D. P. Tsai, L.-Q. Chen, and Y. H. Chu, "Mechanically controllable nonlinear dielectrics", Sci. Adv. **6**, 3180 (2020).